Rock and Soil Mechanics

Volume 43 | Issue 5 Article 7

7-4-2022

Catastrophe prediction of compression-induced fracturing and failure for a tower- shaped unstable rock mass with gentle dip angle

Fu-chuan ZHOU

Hong-mei TANG
hmtang6778@sina.com

Lin-feng WANG

Custom Citation

ZHOU Fu-chuan, TANG Hong-mei, WANG Lin-feng. Catastrophe prediction of compression-induced fracturing and failure for a tower- shaped unstable rock mass with gentle dip angle[J]. Rock and Soil Mechanics, 2022, 43(5): 1341-1352.

Rock and Soil Mechanics 2022 43(5): 1341−1352 ISSN 1000−7598
https: //doi.org/10.16285/j.rsm.2021.6477 rocksoilmech.researchcommons.org/journal

Catastrophe prediction of compression-induced fracturing and failure for a tower-shaped unstable rock mass with gentle dip angle

ZHOU Fu-chuan, TANG Hong-mei, WANG Lin-feng
(Institute of Geotechnical Engineering, Chongqing Jiaotong University, Chongqing 400074, China)

Abstract: The overall failure mode of a tower-shaped unstable rock mass associated with bottom compression-induced fracturing frequently occurs on the steep-high slope with a gentle dip angle in the karst regions, and its damage-catastrophe mechanism belongs to a key issue in the mountainous disaster discipline. Taking a collapse case of Zengziyan unstable rock mass #W12 in Nanchuan District of Chongqing, China, for example, a damage-catastrophe geomechanical model considering the load and the water-weakening effect was built. A damage constitutive equation and a total damage degree evolution equation were derived based on the strain equivalence principle, and the water-weakening function was developed into a cubic function in one unknown for the softening coefficient. Then, the geomechanical model was simplified into an equivalent spring model and the damage-fold catastrophe model was established by the energy balance theory. Finally, the failure criterion and eigenvalue expression of critical displacement mutation for the tower-shaped unstable rock mass were obtained. The results show that when the unstable rock mass #W12 fails, the control variant determining the stability of a fold catastrophe model is –0.003 251, which is less than zero, demonstrating that the system turns into an unstable state. The initial calculated value of the theoretical displacement mutation of 148.70 mm is smaller than the first inflection point of the measured value of 154.34 mm, and the relative error is about 3.65% which tends to be safer. The theoretical damage constitutive curve and evolution curve are consistent with the numerical results obtained in the literature, suggesting that the theoretical model has a good applicability. The research outcome can be applied to predicting the damage evolution process and the eigenvalue of critical displacement mutation for the compression-induced fracturing and failure of a tower-shaped unstable rock mass. It also provides a theoretical basis for monitoring and early-warning of the steep-high unstable rock mass collapse and disaster prevention and mitigation in limestone area.

Keywords: tower-shaped unstable rock mass; compression-induced fracturing and failure; damage mechanics; energy conservation; fold catastrophe model

1 Introduction

The Southwest China has experienced intensive tectonic movement. During this period, the mountain uplift and river incision generated limestone cliff landform with horizontal base, covering an area of more than 50000 km^2, which is a high-risk area of unstable rock mass (URM) collapse disaster[1−2]. The failure mechanism of limestone cliff is very complex, and its failure process is obviously different from that in the sandstone area[3]. Taking the collapse case of Zengziyan URM in Southeast Sichuan as an example, Tang et al.[4−5] deduced the geomorphic evolution process of limestone cliff from the perspective of macro-scale geomorphology and divided the types and influencing factors of tower-shaped compression-induced fracturing and failure. Through the field investigation of 57 collapse disasters in Zengziyan URM area, the calculation method of toppling probability for limestone URM underlying with weak foundation was proposed. He et al.[6] reviewed the research progress of the tower-shaped URM and proposed that the next step should be focused on solving a series of critical scientific problems such as damage-evolution-induced catastrophe, stability analysis controlled by local parts, dynamic disintegration of limestone and its disaster range, and disaster prediction. The URM collapse in limestone strata is also widespread worldwide. For example, Frayssines et al.[7−8] summarized three types of typical failure modes by investigating 25 limestone collapse disasters in the French Alps. Carine et al.[9] used seismic tomography and surface incident radar imaging to study the internal fracture distribution and URM of limestone cliffs in the Northwest Grenoble, France. Oztekin et al.[10] used the geographic information system (GIS) based statistical detachment susceptibility analyses to predict the further aerial extension of the detachment zones of limestone cut slope in the highway of Ankara, Turkey. To sum up, there are many types of URM in limestone areas with complex formation causes. The URM's stability calculation, instability prediction, disintegration and fragmentation, and disaster range need further study.

The tower-shaped URM is widely distributed in the cliff landscape in limestone areas. Powell[11] first reported the tower-shaped rock mass in the Colorado River Basin in the United States. Terzaghi[12] analyzed the tower-shaped rock mass in the Alps. Poisel et al.[13] analyzed three instability modes of tower-shaped rock mass: translational and upright sliding down, rotational

Received: 22 September 2021 Revised: 12 January 2022
This work was supported by the National Natural Science Foundation of China (No. 51678097，No. 5137821).
First Author: ZHOU Fu-chuan, male, born in 1989, PhD candidate, Engineer, focused on disaster prevention and reduction of geotechnical engineering. E-mail: 981480645@qq.com
Corresponding author: TANG Hong-mei, female, born in 1968, PhD, Research fellow, PhD supervisor, mainly engaged in the research on geological disaster reduction theory and prevention technology. E-mail: hmtang6778@sina.com

slide, and toppling. By investigating more than 20 unstable limestone cases in the Three Gorges area of Yangtze River, Chen et al.[14] quantitatively proposed three geometric types of recognition methods from the two aspects of height to thickness ratio and height of the URM. He et al.[6] proposed the formation and influencing factors of tower-shaped unstable limestone. It can be seen that the tower-shaped URM has toppling failure mode, toppling-slumping composite failure mode, and compression-induced fracturing and failure mode[1, 15–16]. The causes of limestone fracturing and failure are multifaceted. From the perspective of deterioration factors, limestone dissolution is the key to the strength reduction of rock mass. The freeze-thaw damage in high-altitude areas has a significant impact. However, from the viewpoint of macro-scale physical properties, it is the strength weakening of rock mass under the action of water, which can be characterized by water-weakening function[14]. From the mechanical point of view, the area at the bottom of the tremendous URM bears heavy load, which has the load damage characteristics of deformation-induced loading with time[17]. The above factors lead to a higher damage degree of limestone at the bottom of the tower-shaped URM and more developed fractures than other parts, which provides storage and flow space for groundwater and further weakens the strength of rock mass at the bottom of the URM. With the continuous accumulation of damage, it will show sudden compression-induced fracturing and failure of a tower-shaped URM.

The stability analysis of the tower-shaped URM in limestone areas has been reported in the literature [18], but it still lacks the instability prediction method. Most rock mechanics and geoscience problems are strongly nonlinear. The nonlinear theory developed in the 1970 s has become a powerful mathematical tool to solve the problems of complex nonlinear systems[19]. The total potential energy function is established according to the energy balance principle, and some standard models of elementary catastrophe theory are obtained through mathematical transformation. Then the system catastrophe instability criterion is established according to the control variables. It has been widely used in the fields of the slope, URM, and other geosciences[20–25]. Therefore, the sudden compression-induced fracturing and failure of the tower-shaped URM can be predicted based on the catastrophe theory.

Based on the Zengziyan tower-shaped URM collapse in Nanchuan District, Chongqing, China, this paper intends to establish a comprehensive quantitative analysis method for instability prediction under multiple disciplines, such as geomechanics, continuous damage mechanics, energy balance principle, and fold catastrophe model. By constructing the damage catastrophe model under the coupling of load damage factor and water-weakening effect, this paper puts forward a compression-induced fracturing and failure criterion for the tower-shaped URM based on a physico-mechanical process, reveals the scientific problem of damage-evolution-induced catastrophe of the tower-shaped URM, and provides a theoretical basis for monitoring and early warning of the URM collapse, disaster prevention and mitigation in limestone area.

2 Geological background

2.1 Geological conditions of the cliff

Zengziyan URM groups are located in Yuquan Village, Jinshan Town, Nanchuan District, Chongqing. It is located in the east wing of the near axis of the middle section of Jinfo mountain syncline and close to the east of the Nanchuan aluminum mine. At about 12:51 on August 12, 2004, the URM #W12 collapsed, and about 500000 m^3 of the URM collapsed and disintegrated. The slope within an area of nearly 2 km^2 was covered with fragmented rocks and the dust covered the sky of about 3 km^2 for more than 40 min[26]. The collapse process is shown in Fig.1.

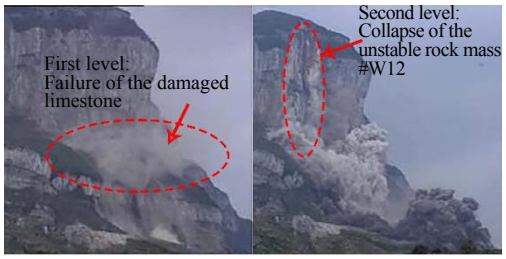

(a) Before collapse (b) During collapse

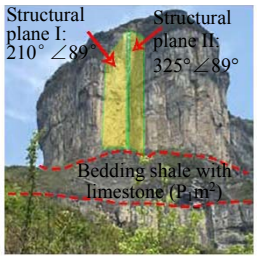

(c) After collapse

Fig. 1 Collapse process photographs of Zengziyan URM #W12

Zengziyan rock mass is composed of two-stage cliff from top to bottom, with typical binary mountain structural characteristics of "steep and hard on the upper part, and gentle and soft on the lower part"[4] (Fig.2). The second-level cliff is composed of limestone from Members 3, 4 and 5 of the lower Permian Maokou Formation (P_1m^{3+4+5}), with an altitude of 1550–1814 m and a cliff height of 200–215 m. The base is the slope terrain of limestone sandwiched between shale in Member 2 of the lower Permian Maokou Formation (P_1m^2), with an altitude of 1500–1550 m and a slope angle of 30°–52°. The first-level cliff comprises limestone including Member 1 of the Maokou Formation (P_1m^1) and the Qixia Formation (P_1q), with an altitude of 1400–1545 m and a cliff height of 80–105 m. Its base is a slope terrain composed of bauxite of the Liangshan Formation (P_1l) and silty shale of middle Silurian Hanjiadian Formation (S_2h), with a slope angle of 18°–26°.

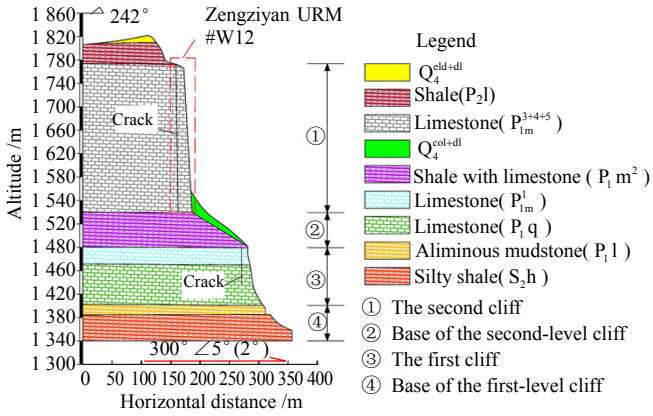

Fig. 2 Geological profile of Zengziyan URM #W12

2.2 Geological model of the URM

The URM #W12 is located on the second-level cliff, in a triangular prism shape, with a height of about 240 m, a width of about 32 m, a length of about 64 m, and a shear-outlet elevation of about 1560 m. The lithology is limestone of the Members 3–5 of the Maokou Formation, which is classified as hard rock. Three groups of structural planes have developed in the rock mass, of which two groups of vertical and orthogonal fractures penetrating from top to bottom, with a length of about 200 m and a width of 3–10 m. The other group is near horizontal. The underlying horizontal layered base is about 40 m thick. The lithology is the black thin medium-thick layered calcareous talcous shale, interbedded with dark gray thin to medium-thick layered silty biological microcrystalline limestone. The drilling data[27] reveal that the rock core at the lower part of the URM #W12 is relatively broken to relatively complete and locally fragmented. Under the coupling effects of fissure water, weathering, temperature change, biological root splitting, artificial mining, and other factors, it shows a compression-induced failure mode of the tower-shaped URM.

From the monitoring of the failure process, it is found that the URM's bottom is the accumulation and circulation area of water. It is also the part with the maximum stress and the most significant strength reduction of the URM, which is called the limestone deterioration area. Under the gravity of the rock mass in the upper incomplete deterioration area, the fracturing and fragmentation of the rock in the deterioration area is the root cause of the overall seating of the URM, as shown in Fig.3(a). The reasons include the following aspects:

(1) With the damage evolution in the deterioration area, the effective contact area decreases, the effective stress increases gradually, and the strain increases. It is similar to the rheological phenomenon with time, but it is essentially a load damage effect.

(2) Zengziyan rock mass is in an acid corrosive environment. The shale intercalated with limestone of the base rock mass is an excellent water-proof layer. Under the coupling effect of acidic water and stress, the cracks in the URM's deterioration area continue to propagate and coalesce, and the strength of the rock mass decreases significantly, indicating a water-weakening effect.

The strength of the rock mass in the limestone deterioration area continues to reduce under the loading and water-weakening effect. When the strength decreases to a critical value, it presents a sudden compression-induced fracturing and failure phenomenon. The geological model can be established according to the field situation, as shown in Fig.3(b).

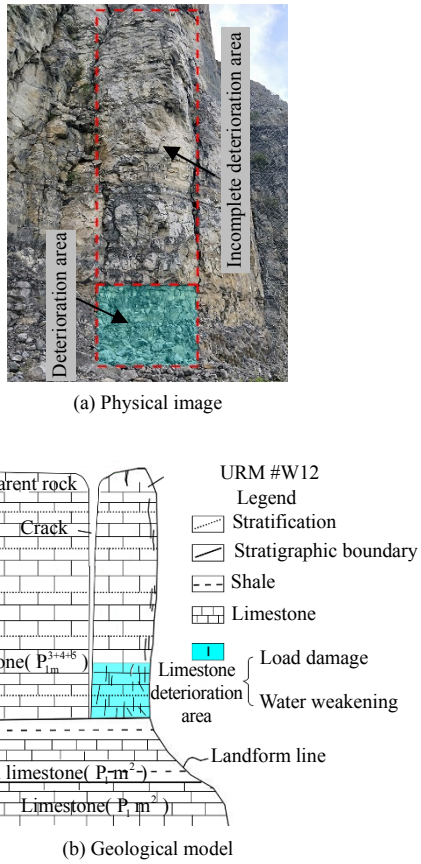

Fig. 3 Geological model of Zengziyan URM #W12

3 Damage constitutive equation

3.1 Multi-factor coupling damage constitutive equation

Lemaitre[28] extracted the voxel from the damaged body and defined the cross-sectional area of the surface element along direction n' on the voxel as A, the area occupied by the randomly distributed microcracks and holes on the surface is A_D, and the effective support area is A' (Fig. 4). Based on this, the damage factor D_n is defined:

$$D_n = \frac{A_D}{A} = \frac{A - A'}{A} \quad (1)$$

where the damage variable D_n is the proportion of the defects in a certain state, which can characterize the degree of defects.

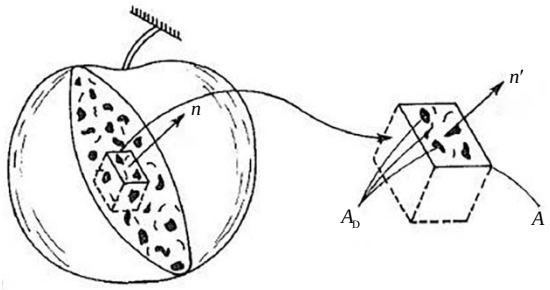

Fig. 4 Damage model of an element[28]

Using the strain equivalence theory[28] and its generalized theory[29], the micromechanics and macro-mechanics can be linked, and its core is to establish three basic equations, i.e.

$$\sigma^{(1)}A_1 = \sigma^{(2)}A_2 \tag{2}$$

$$\varepsilon^{\mathrm{e}} = \frac{\sigma^{(1)}}{E_2} = \frac{\sigma^{(2)}}{E_1} \tag{3}$$

$$D_2 = \frac{A_1 - A_2}{A_1} \tag{4}$$

where $\sigma^{(i)}$, A_i and E_i are the effective stress (MPa), effective area (m^2) and effective elastic modulus (MPa) under the ith damage state, respectively, and i = 1 or 2; ε^{e} is the equivalent effective strain; D_2 is the incremental damage proportion of the second damage state compared to the first damage state.

Equation (2) is the assumption of constant internal force, which means that the stress may change under the influence of different damage factors at a constant external load, but the resultant internal force is constant and balanced with the external load.

Equation (3) is the generalized strain equivalence equation, which indicates that the strain obtained by the effective stress in the first damage state acting on the elastic modulus in the second damage state is equivalent to that obtained by the effective stress in the second damage state acting on the elastic modulus in the first damage state.

Equation (4) is the damage variable, which means that adding the second damage to the first damage state will generate new defects, and the proportion of the new defect area is defined as D_2.

Combining Eqs. (2) and (4), we obtain

$$\sigma^{(2)} = \frac{\sigma^{(1)}}{1 - D_2} \tag{5}$$

Combining Eqs. (3) and (5), we have

$$E_2 = E_1 \frac{\sigma^{(1)}}{\sigma^{(2)}} = E_1\left(1 - D_2\right) \tag{6}$$

The damage constitutive equation under the coupling effect of the two damage states can be obtained by multiplying the strain $\varepsilon^{(2)}$ in the second damage state at the two sides of Eq. (6):

$$\sigma^{(2)} = E_1\left(1 - D_2\right)\varepsilon^{(2)} \tag{7}$$

Similarly, according to the recursive analysis, the damage constitutive equation under the third to nth damage coupling state can be expressed as

$$\sigma^{(n)} = E_1\varepsilon^{(n)}\prod_{k=1}^{n}\left(1 - D_k\right) \tag{8}$$

where $\sigma^{(n)}$ and $\varepsilon^{(n)}$ are the stress and strain under the action of n damage factors, respectively; k represents the kth damage factor; and D_k is the damage degree caused by the k^{th} damage factor. It should be pointed out that during the derivation of the multi-factor coupling damage equation, in order to express and reveal the law conveniently, n types of damage factors are set, and it is assumed that the latter damage factor is the result of superposition based on the former damage factor, but in practice, it is difficult to judge the order of damage factors, which can occur randomly or synchronously, while the stress–strain curve is a continuous change process. No matter what type of damage occurs, in essence, it is to reduce the stiffness of the stress–strain curve (change the nonlinear trend), which can be characterized by introducing the damage factor. Therefore, the damage constitutive equation under multi-factor coupling has the following general form:

$$\sigma = E_0\varepsilon\prod_{k=1}^{n}\left(1 - D_k\right) \tag{9}$$

where E_0 is the initial elastic modulus of intact rock (MPa); σ is the stress (MPa); and ε is the strain.

The total damage degree D under multi-factor coupling can be expressed as

$$D = 1 - \prod_{k=1}^{n}\left(1 - D_k\right) \tag{10}$$

3.2 Damage constitutive equation of URM #W12

In this section, the damage factors of the URM #W12 are analyzed firstly, and then substituted into the damage constitutive equation and total damage degree equation with the general form in section 3.1.

The deterioration of the rock mass quality is a quantitative change process that the rock mass macro-damage is accumulated by the micro-unit failure. The damage evolution has the effect of "one increases and the other decreases", i.e. all kinds of damage lead to the decrease of rock mass strength (decrease of bearing capacity). At the same time, when the external load is determined, due to the reduction of the actual support area, the internal effective stress continues to increase, resulting in a phenomenon of "loading". Therefore, the damage effect is a mechanical evolution way to change the macro-mechanical properties of rock mass through "one increases and the other decreases".

3.2.1 Load damage factor of limestone

Load damage is a kind of damage factor with "loading" characteristics. The damage initiates from the weak element, while the defects formed during the diagenetic process of the geological body are complicated and random. The random distribution of the load damage has been widely studied from the perspective of statistics, which can be expressed as[30]:

$$D_{\mathrm{L}} = 1 - \mathrm{e}^{-(\varepsilon/\varepsilon_0)^m} \tag{11}$$

where D_{L} is the load damage degree, which is a negative exponential function of strain ε; m and ε_0

are the Weibull's double parameters.

3.2.2 Water-weakening effect of limestone

There are many damage variables resulting in the reduction of limestone strength, such as karst dissolution, freeze-thaw, and other water-related damage factors. This kind of damage is generally analyzed from a micro-scale perspective, and it is difficult to evaluate the physico-mechanical properties of the macroscopic rock mass in practice. In order to reflect the damage effect of the environmental water, the water-weakening function is usually introduced to characterize the weakening phenomenon of the rock mass strength. It should be pointed out that the damage degree reflects the defect proportion in a material, while the water-weakening function reflects the effective action proportion, and the sum of both is equal to 1.

The conventional water-weakening function[31] is a binary quadratic equation (Eq. (12)) about the degree of saturation S_r and softening coefficient R. The softening coefficient is regarded as a constant theoretically. In fact, different degrees of saturation corresponds to different rock strengths and softening coefficients[32]. Therefore, the softening coefficient is not a constant and needs to be improved. The binary functions can be transformed into univariate functions by dimensionality reduction:

$$f(R, S_r) = (1-R)(1-S_r)^2 + R \tag{12}$$

$$R = \frac{\sigma_b^n}{\sigma_b^d} \tag{13}$$

$$R_{sat} = \frac{\sigma_b^{sat}}{\sigma_b^d} \tag{14}$$

$$R = (R_{sat} - 1)S_r + 1 \tag{15}$$

Equation (13) is a function of softening coefficient R, which represents the ratio of uniaxial compressive strength (UCS) σ_b^n of natural rock to dry UCS σ_b^d. Equation (14) is a function of the saturation softening coefficient R_{sat}, which represents the ratio of saturated UCS σ_b^{sat} to dry UCS σ_b^d. Equation (15) represents the linear relationship between softening coefficient R and degree of saturation S_r. When the rock is fully saturated ($S_r = 1$), the rock softening coefficient R is equal to the saturation softening coefficient R_{sat}. When the rock is dry ($S_r = 0$), the rock is not softened ($R = 1$).

Combining Eqs. (12) and (15), we obtain

$$f(R) = (1-R)\left(\frac{R_{sat} - R}{R_{sat} - 1}\right)^2 + R \tag{16}$$

The water-weakening function shown in Eq. (16) is a univariate cubic function of softening coefficient R, $R \in [R_{sat}, 1]$, $f(R) \in [R_{sat}, 1]$. The existing binary water-weakening function is simplified to a univariate cubic water-weakening function. The R and R_{sat} can be solved by Eqs. (13) and (14), and substituted into Eq.(16). Finally, the value of water-weakening function under certain natural moisture content can be obtained, which simplifies the parameters required for laboratory test and has a clear physical meaning.

The damage degree D_w caused by the environmental water has the following relationship with the value of water-weakening function $f(R)$:

$$D_w = 1 - f(R) \tag{17}$$

3.2.3 Damage constitutive model and total damage degree of limestone

Substituting Eqs. (11), (16) and (17) into Eq. (9), the total damage constitutive model under the coupling effect of load and water-weakening can be obtained:

$$\sigma = \left[(1-R^l)\left(\frac{R_{sat}^l - R^l}{R_{sat}^l - 1}\right)^2 + R^l\right] e^{-(\varepsilon/\varepsilon_0)^m} \cdot E_0^l \varepsilon \tag{18}$$

where R^l is the softening coefficient of limestone; R_{sat}^l is the saturation softening coefficient of limestone; and E_0^l is the initial elastic modulus of limestone (MPa).

Substituting Eqs. (11), (16) and (17) into Eq. (10), the total damage degree D^l of limestone deterioration area can be obtained as

$$D^l = 1 - \left[(1-R^l)\left(\frac{R_{sat}^l - R^l}{R_{sat}^l - 1}\right)^2 + R^l\right] e^{-(\varepsilon/\varepsilon_0)^m} \tag{19}$$

According to the geometric conditions of the total damage constitutive curve of limestone[30], we have

$$\sigma\Big|_{\varepsilon=\varepsilon_f^l} = f(R^l) \cdot E_0^l \ \varepsilon_f^l \cdot e^{-\left(\varepsilon_f^l/\varepsilon_0\right)^m} = \sigma_f^l \tag{20}$$

$$\frac{d\sigma}{d\varepsilon}\Big|_{\varepsilon=\varepsilon_f^l} = \left[1 - m\left(\frac{\varepsilon_f^l}{\varepsilon_0}\right)^m\right] f(R^l) \cdot E_0^l \cdot e^{-\left(\varepsilon_f^l/\varepsilon_0\right)^m} = 0 \tag{21}$$

where $f(R^l)$ is the value of water-weakening function of the limestone; σ_f^l is the peak stress of the total damage constitutive curve of the limestone (MPa); and ε_f^l is the peak strain of the total damage constitutive curve of the limestone.

The Weibull's double-parameter analytical formulae can be quantitatively obtained by combining Eqs. (20) and (21):

$$m = \frac{1}{\ln[f(R^l) \cdot E_0^l \cdot \varepsilon_f^l / \sigma_f^l]} \tag{22}$$

$$\varepsilon_0 = \varepsilon_f^l \cdot m^{1/m} \tag{23}$$

4 Mechanical evolution of the compression-induced fracturing and failure

4.1 Mechanical evolution process

According to Fig.3(b), the URM #W12 is completely isolated from the parent rock by the deep fissure from the rear part of the URM to the base. The URM's bottom is the deterioration area, and the middle and upper parts are the incomplete deterioration areas. Under the action of the deadweight of the incomplete deterioration area, the deterioration area was fractured by compression, and the upper incomplete deterioration area without support continues to collapse. The failure process of the limestone deterioration area is similar to the uniaxial compression test[33]. Based on this, a simplified mechanical model of the URM is established (Fig.5(d)).

In Fig.5(d), ABC_2D_2 is the deterioration area, which

is in uniaxial compression state. D_2C_2EF is the incomplete deterioration area, which has a pressure effect on the deterioration area. The variable B is the width of the URM (m); H is the height of the URM (m); $H_1(t)$ is the height of the incomplete deterioration area (m), which is a function of time t; $H_2(t)$ is the height of deterioration area (m); $W(t)$ is the deadweight of the incomplete deterioration area (kN); $F(t)$ is the shear resistance of the rock bridge (kN); and $N(t)$ is the supporting force of the deterioration area (kN).

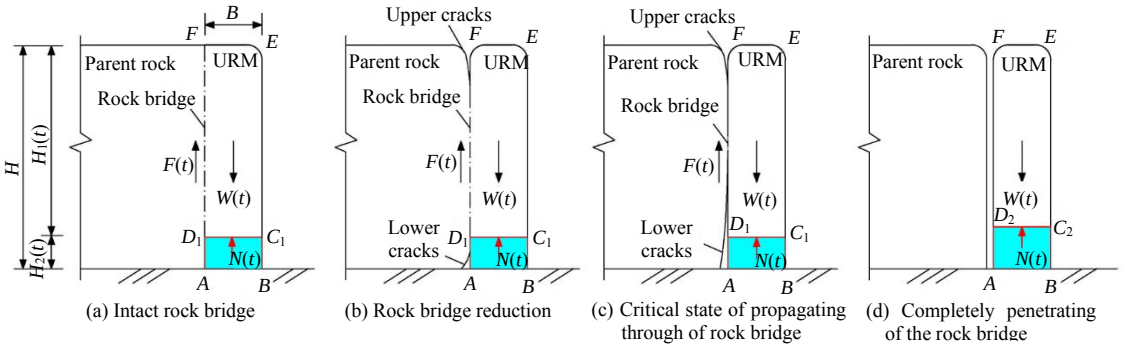

(a) Intact rock bridge (b) Rock bridge reduction (c) Critical state of propagating through of rock bridge (d) Completely penetrating of the rock bridge

Fig. 5 Simplified mechanical model

4.2 Equivalent spring model

4.2.1 Static equilibrium and deformation compatibility equation

The following assumptions are made:

(1) Before the rock bridge at the rear of the tower-shaped URM has completely penetrated (Fig.5(a)–5(c)), the deadweight $W(t)$ of the incomplete deterioration area is shared by the supporting force $N(t)$ of the deterioration area and the rock bridge shear resistance $F(t)$. With the crack propagation, the rock bridge is cut through (Fig.5(d)), the shear resistance $F(t)$ of the rock bridge is gradually reduced to 0, and the deadweight $W(t)$ is borne by the $N(t)$ in the deterioration area. The deadweight of the incomplete deterioration area has a loading effect that increases with time on the deterioration area.

(2) After the large fractures are connected, the internal fissures of the deterioration area ABC_2D_2 are continuously developed, the vertical deterioration range rises from C_1D_1 to C_2D_2, and the volume of the incomplete deterioration area decreases (Fig.5(d)), resulting in the unloading mechanism that the gravity applied to the deterioration area decreases with time. However, the fracturing and fragmentation degree of the rock mass in the deterioration area become higher, which has entered the strain-softening stage, and sudden compression-induced fracturing and failure may occur.

(3) The equivalent spring model is regarded as a system. In the mechanical analysis, the vertical deformation is mainly considered, and the horizontal transverse deformation is neglected. The incomplete deterioration area (loading area) is always in an elastic state during loading process, and the stiffness $k_m = \tan\alpha$, where α is the inclination angle (°) of the slope for the linearly elastic section in the incomplete deterioration area. The deterioration area has experienced elastic deformation stage, stable fracture stage and unstable fracture stage in the rock bridge connection process (loading process). After the rock bridge is cut through, the deterioration area enters the nonlinear softening stage and failure stage. The nonlinear softening stage has an inflection point, and the sudden instability occurs in the nonlinear softening section.

Based on the simplified mechanical model (Fig.5(d)), the incomplete deterioration area is equivalent to a spring with stiffness k_m. The deadweight $W(t)$ of the URM is loaded on the end of the spring (regarded as the loading area), resulting in the full displacement u_w, and the deterioration area produces compression deformation u, as shown in Fig.6. Before loading, the contact surface is located at the position shown in D_2C_2 (Fig.6(a)); and after loading, the contact surface moves to D_2' C_2' position (Fig.6(b)). Selecting the contact surface D_2' C_2' for analysis, the limestone deterioration area is subjected to the force $f(u)$ and the spring is subjected to the reaction force $N(t)$, as shown in Fig.6(c).

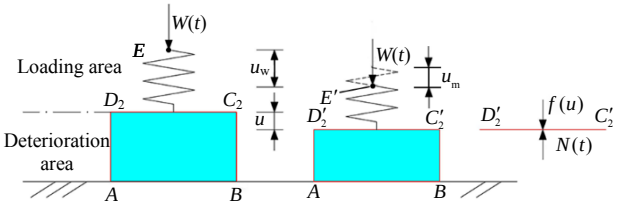

(a) Before loading (b) After loading (c) Force on the contact surface

Fig. 6 Equivalent spring model

Assuming that the compression deformation value of the equivalent spring under the action of the deadweight is u_m, the total displacement at the end of the spring is equal to the sum of the compression deformation values of the spring and the complete deterioration area, i.e. the equivalent spring model satisfies the following deformation compatibility equation:

$$u_w = u_m + u \tag{24}$$

The static equilibrium equation is written as

$$W(t) = f(u) = N(t) = k_m u_m \tag{25}$$

The relationship between stiffness and elastic modulus

under uniaxial pressure mode is written as

$$k_{\mathrm{m}}=\frac{E_0^{\mathrm{l}}B}{H_1(t_{\mathrm{d}})} \tag{26}$$

where the displacement u of the deterioration area under the action of $f(u)$ reflects the constitutive relationship of the limestone deterioration area; and $H_1(t_{\mathrm{d}})$ is the height of the incomplete deterioration area (m) at the time t_{d} of rock bridge penetration.

4.2.2 Transformation of damage constitutive equation

According to the geometric dimensions shown in Fig.5(a) and the geometric relationship between strain and displacement, the stress–strain damage constitutive equation of the deterioration area shown in Eq. (18) is transformed into the damage constitutive equation in the form of force–displacement:

$$f(u)=f(R^{\mathrm{l}})\cdot \mathrm{e}^{-(u/u_0)^m}\cdot k_{\mathrm{m}}u \tag{27}$$

$$u_0=u_{\mathrm{c}}^{\mathrm{l}}\cdot m^{1/m} \tag{28}$$

$$u_{\mathrm{c}}^{\mathrm{l}}=\varepsilon_{\mathrm{f}}^{\mathrm{l}}\cdot H_2(t_{\mathrm{d}}) \tag{29}$$

where $u_{\mathrm{c}}^{\mathrm{l}}$ is the peak displacement of limestone in the deterioration area (m); u_0 is the converted displacement (m); $f(R^{\mathrm{l}})$ is the water-weakening function of limestone; $H_2(t_{\mathrm{d}})$ is the height of the deterioration area (m) at the time t_{d} when the rock bridge propagates through, and the height of the deterioration area can be dynamically adjusted according to the actual situation.

According to the assumption (3) in section 4.2.1, the constitutive models of the incomplete deterioration area and deterioration area can be drawn (Fig.7). The constitutive curve of deterioration area is shown on the $f(u)$–u curve on the right side of Fig.7. It comprises the linear elastic section and nonlinear strengthening section before peak point *c*, and nonlinear softening section after point *c*. The softening section after the peak has the important characteristics of an inflection point *t*. The incomplete deterioration area is shown on the left side of Fig.7. It is always in a linear elastic state within the load $f(u_c)$.

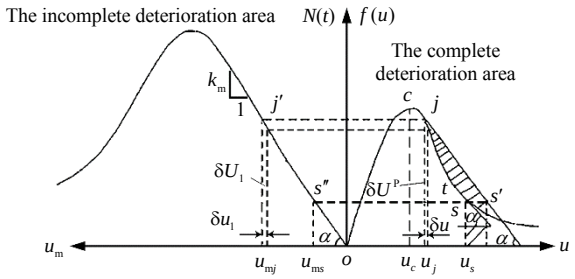

Fig. 7 Constitutive curves of incomplete and complete deterioration areas[34]

The dynamic instability of the system occurs in the post-peak softening section of the deterioration area. When a small displacement increment $\delta u\ (>0)$ is generated on the softening section of the curve $f(u)$, the micro-cracks propagate in the deterioration area, further deformation consumes energy, and the energy to be absorbed is $\delta U^{\mathrm{P}}=f(u)\cdot\delta u$. With the decrease of $f(u)$, the unloading displacement $\delta u_{\mathrm{l}}\ (<0)$ appears in the incomplete deterioration area, and the elastic deformation energy released by unloading is $\delta U_{\mathrm{l}}=N\cdot\delta u_{\mathrm{l}}\ (<0)$. When $-\delta U_{\mathrm{l}}<\delta U^{\mathrm{P}}$, the work δW needs to be done by an external force to make the complete deterioration area continue to deform. The points *j* and *s* on the softening section of the complete deterioration area correspond to the starting point and ending point of dynamic fracture at the quasi-static stage of the system, respectively. The horizontal line passing through the two points intersects the curve of the incomplete deterioration area at the points j' and s''. u_j and u_s correspond to the lower and upper limits of critical fracture displacement, respectively. The linear elastic section of the incomplete deterioration area is translated to the right side, which intersects the nonlinear softening section of the complete deterioration area at point *j*. The horizontal line crossing point *s* intersects the straight line of the elastic section in the incomplete deterioration area after moving to the right side at point s'. Then the shaded area represents the part of the elastic deformation energy released by the incomplete deterioration area that exceeds the energy dissipation required for the deformation of the deterioration area.

For the arbitrary deformation value u_j on the curve $f(u)$ of complete deterioration area, the unique compression deformation value $u_{\mathrm{m}j}$ of spring can be obtained from the static equilibrium equation (Eq. (25)):

$$u_{\mathrm{m}j}=N_j/k_{\mathrm{m}}=f(u_j)/k_{\mathrm{m}} \tag{30}$$

According to the deformation compatibility equation (Eq. (24)), there is a unique total displacement $u_{\mathrm{w}j}$:

$$u_{\mathrm{w}j}=u_{\mathrm{m}j}+u_j=f(u_j)/k_{\mathrm{m}}+u_j \tag{31}$$

It can be seen that the spring's compression deformation variable $u_{\mathrm{m}}(u)$ and the total displacement $u_{\mathrm{w}}(u)$ are functions of the deformation variable u in the deterioration area.

4.3 Total potential energy function and fold catastrophe model

For the rock mass fracture of the equivalent spring model under uniaxial compression, the total potential energy function Π of the system is written as

$$\Pi=\int_0^u f(u)\mathrm{d}u+\frac{1}{2}k_{\mathrm{m}}u_{\mathrm{m}}^2(u)-\int_0^{u_{\mathrm{w}}(u)}W(u_{\mathrm{w}})\mathrm{d}u_{\mathrm{w}} \tag{32}$$

where $W(u_{\mathrm{w}})$ is the work done by the deadweight of the incompletely deterioration area of the URM along the direction of total displacement u_{w}.

The energy input rate J is defined as[34]:

$$J=W(u_{\mathrm{w}})\frac{\mathrm{d}u_{\mathrm{w}}(u)}{\mathrm{d}u} \tag{33}$$

Taking the derivative of Eq. (32) with respect to the displacement *u*, we have

$$\frac{\mathrm{d}\Pi}{\mathrm{d}u}=f(u)+k_{\mathrm{m}}u_{\mathrm{m}}\frac{\mathrm{d}u_{\mathrm{m}}(u)}{\mathrm{d}u}-W(u_{\mathrm{w}})\frac{\mathrm{d}u_{\mathrm{w}}(u)}{\mathrm{d}u} \tag{34}$$

In Eq. (30), u_j is the arbitrary deformation value, which can also be replaced with any symbolic variable u. Taking the derivative of Eq. (30) with respect to the displacement u, we have

$$\frac{\mathrm{d}u_{\mathrm{m}}(u)}{\mathrm{d}u} = f'(u)/k_{\mathrm{m}} \tag{35}$$

Substituting Eqs. (25), (33) and (35) into Eq. (34), we have

$$\frac{\mathrm{d}\Pi}{\mathrm{d}u} = f(u) + f(u)f'(u)/k_{\mathrm{m}} - J \tag{36}$$

Literature[34] pointed out that the energy input rate J is an index that judges the instability of the system. When $J=0$, even if there is no external force applied, the system can fail abruptly by its own energy accumulation and transfer.

Let Eqs. (33) and (36) equal 0, the quasi-static equilibrium equation of the system can be obtained as

$$\frac{\mathrm{d}\Pi}{\mathrm{d}u} = f(u) + f(u)f'(u)/k_{\mathrm{m}} = 0 \tag{37}$$

Obviously, according to the catastrophe theory, the differential equation (Eq. (37)) of the total potential energy function of the system is a catastrophe manifold. Equation (27) is substituted into Eq. (37), and the Taylor expansion is made at the displacement inflection point u_t of the softening section on $f(u)$ curve. Figure 8 shows the flow chart for solving the fold catastrophe model.

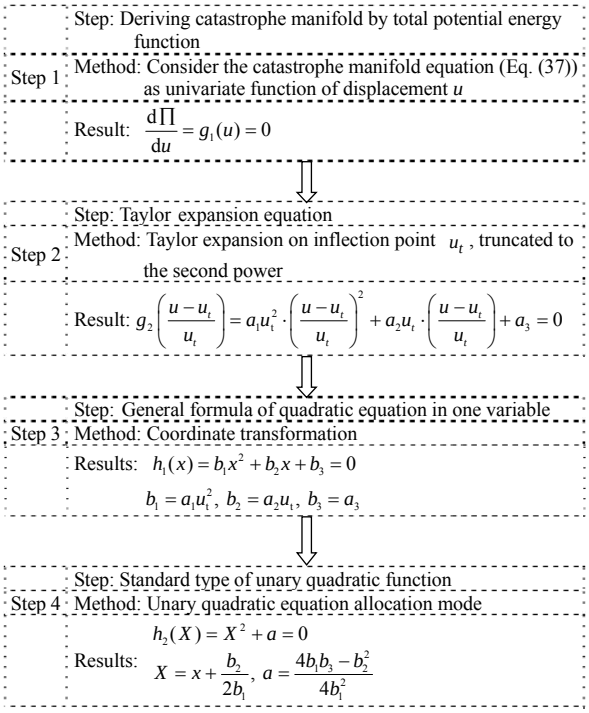

Fig. 8 Solving flow chart of fold catastrophe model

In step 1 of Fig.8, the total potential energy function (Eq. (37)) is obtained through the energy balance principle, which is related to the damage constitutive equation $f(u)$ and its first-order derivative $f'(u)$. Let Eq. (37) equal $g_1(u)$.

Step 2 means that the Taylor expansion is made at the displacement inflection point u_t on the total potential energy function and truncated to the second power term to obtain the general formula of the univariate quadratic equation, where a_1, a_2 and a_3 are the functions of water-weakening function $f(R^1)$, displacement inflection point u_t, converted displacement u_0, Weibull's parameter m, spring stiffness k_{m} and other parameters. Given the above parameters, the variables $a_1[f(R^1), u_t, u_0, m, k_{\mathrm{m}}]$, $a_2[f(R^1), u_t, u_0, m, k_{\mathrm{m}}]$ and $a_3[f(R^1), u_t, u_0, m, k_{\mathrm{m}}]$ can be obtained.

Step 3 is the first coordinated transformation process. Its function is to simplify the equation formally, which is convenient to extract the equation coefficients for calculation during programming. b_1, b_2 and b_3 are the equation coefficients that can be obtained.

Step 4 is the second coordinate transformation process, which transforms the general formula of univariate quadratic equation into standard form, i.e. the mathematical form of fold catastrophe model. The important output parameters of the fold model are written as follows:

$$X = x + \frac{b_2}{2b_1} \tag{38}$$

$$x = \frac{u-u_t}{u_t} \tag{39}$$

$$u_t = u_0\cdot\left(1+\frac{1}{m}\right)^{\frac{1}{m}} \tag{40}$$

$$a = \frac{4b_1b_3 - b_2^2}{4b_1^2} \tag{41}$$

where X is the state variable of the fold catastrophe model; a is the control variable; and x is the normalized variable of displacement u.

In the fold catastrophe model (Fig.9), when the control variable $a>0$, the system is empty. When $a=0$, the system is in an asymptotic state. When $a<0$, there are two state variables x_j and x_s in the system. x_j of lower branch 1 is in unstable state and x_s of upper branch 2 is in stable state. The transition process of state variable from x_j to x_s indicates system instability[35]. Therefore, by controlling the value of variable a, we can judge whether the system will fail or not and predict when it will be unstable according to calculation results of x_j.

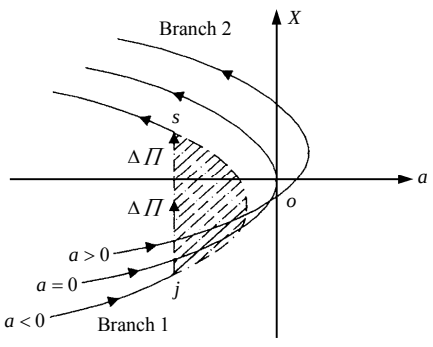

Fig. 9 Equilibrium surface of the fold catastrophe model[35]

Combining with Cook stiffness criterion[36], the system will fail when following conditions are met:

$$f'(u)+k_{\mathrm{m}}=0 \tag{42}$$

The first-order derivative of Eq. (27) is substituted into Eq. (42). The displacement eigenvalues u_j and u_s of sudden instability of the univariate nonlinear equation can be obtained using the implicit function method of the numerical software. Alternatively, the displacement eigenvalue can be obtained by the inverse solution method. Specifically, the displacement inflection point u_t and the control variable a can be obtained using Eqs. (40)—(41), then the state variable X can be obtained using the mathematical standard form of the fold catastrophe model in Step 4 of Fig. 8, and the standardized variable x of displacement u can be obtained by Eq. (38). Finally, the characteristic displacements u_j and u_s can be obtained by Eq. (39):

$$u=\begin{cases}u_t\left(1-\dfrac{b_1}{2a_1}+\sqrt{-a}\right)\\ u_t\left(1-\dfrac{b_1}{2a_1}-\sqrt{-a}\right)\end{cases} \tag{43}$$

In Eq. (43), under the geological conditions at a certain time, all the variables on the right side of the equation can be obtained. When the constant term of the standard form of the univariate quadratic equation $a<0$, it has two unequal real roots, which shows that under the geometric conditions and physicomechanical properties at this time, there is the starting and ending points of rock fracture with sudden instability in the system. When $a=0$, there is only one real root, and the system is in a gradual change state. When $a>0$, it has two complex roots, and the system does not satisfy the condition of sudden instability.

The above analysis process can be realized by compiling a calculation program with Matlab numerical software.

5 Prediction analysis

The Zengziyan URM #W12 and adjacent URMs #W29 and #W23 are in the same stratigraphic era and possess the same lithology. Referring to the parameters reported in the *Construction Drawing Design of W29 and W23 Unstable Rock Mass Treatment Project of Zengziyan Rock in Jinfo Mountain, Nanchuan District, Chongqing*[37], the dry, natural and saturated UCS values of limestone are 56, 51.17, 42.07 MPa, respectively, and the initial elastic modulus $E_0^1=43.68$ GPa. Referring to the relevant test results[38], the peak stress of limestone $\sigma_{\mathrm{f}}^1=120$ MPa, the peak strain $\varepsilon_{\mathrm{f}}^1=0.003$, the URM's height $H=240$ m, the incomplete deterioration area's height $H_1=192$ m, the deterioration area's height $H_2=48$ m, and the URM's width $B=32$ m.

The above data are input into the damage fold catastrophe model function file written by Matlab to obtain the intermediate parameters and prediction parameters, as shown in Table 1.

Table 1 Damage catastrophe prediction model's output of the tower-shaped URM

Intermediate parameters						Prediction parameters			
$f(R)$	m	ε_0	u_0 /mm	u_c /mm	u_t /mm	a	Condition	u_j /mm	u_s /m
0.9506	26.81	3.39×10^{-3}	162.79	144	163.02	–0.003251<0	Unstable condition	148.7	267.2

The predictive control variable $a=-0.003251<0$ indicates that the system is in an unstable state and may have a sudden instability mode. The displacement of the complete deterioration area reaches the fracture starting point $u_j=0.1487$ m, the URM system enters the strain-softening section and will suddenly jump to the rupture termination point $u_s=0.2672$ m which specifies that brittle fracturing and failure will occur rapidly once the URM system reaches the fracture starting point. This phenomenon is consistent with the instability characteristics of rock collapse without significant displacement signs.

Figure 10 shows the accumulative deformation of the URM #W12 continuously observed at the site monitoring point #7 from March 8 to August 12, 2004. The first inflection point appeared on July 19, and the accumulative deformation was about 154.34 mm. The second inflection point appeared on August 11, and the accumulative deformation was 298.3 mm. The fracturing and failure occurred at noon of August 12[26].

The comparison between the theoretically predicted value and the field measured value is listed in Table 2. It is shown that the theoretical values of the fracture starting point, fracture ending point and origin-destination distance are less than the measured values, in which the absolute error accuracies of the failure ending point and origin-destination distance are at cm level. The absolute error accuracy of the failure starting point is at mm level. The relative errors of the fracture starting point, fracture ending point and origin- destination distance are 3.65% (less than 5%), 10.43% and 17.69%, respectively.

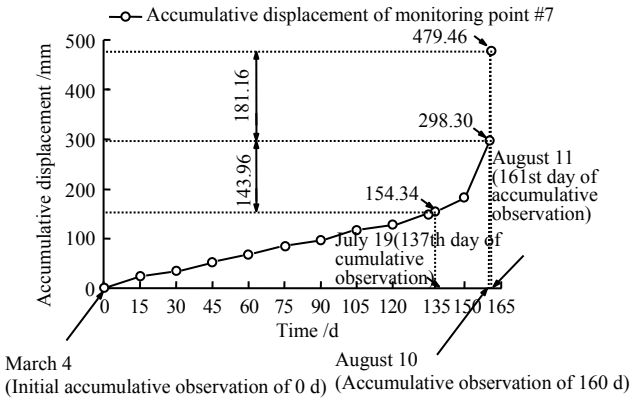

Fig. 10 Time–history curve of field measured displacement for the URM #W12

Table 2 Error comparison between theoretical and measured values

Item	Theoretical value /mm	Measured value /mm	Absolute error /mm	Relative error /%
Fracture starting point u_i	148.70	154.34	–5.64	–3.65
Fracture ending point u_s	267.20	298.30	–31.10	–10.43
Origin-destination distance	118.50	143.96	–25.56	–17.69

Note: The absolute error equals the absolute subtraction between theoretical value and measured value, and the relative error equals

$$\frac{\text{Theoretical value-measured value}}{\text{measured value}}\times 100\%$$

The reasons for the large errors of the fracture ending point and the origin-destination distance are as follows:

(1) In the calculation of relative error in percentage, because the magnitudes of theoretical value and measured value is at dm level, when the absolute error accuracies are controlled at mm level, the relative errors can be basically guaranteed to be within 5%. However, the theoretical solution in this paper is still difficult to ensure that all predicted values are at the mm level, but basically reach the cm level.

(2) Although the absolute errors of the fracture ending point and the origin-destination distance are of the same magnitude, the relative errors are quite different. Because when the numerator (absolute error) of the relative error is similar, its denominator (measured value) has a great influence on the results.

(3) The predicted results are closely related to the value of Weibull's parameter *m*. The larger the *m* is, the steeper the curve at the softening stage is, and the smaller the displacement difference between the starting point and the ending point of rock fracture is. The *m* value is related to water-weakening function, rock elastic modulus, peak stress, strain, and other factors. The difference between laboratory and field will lead to the deviation of calculation results for *m*, further resulting in the deviation of the predicted fracture starting point and ending point.

(4) The displacement of the fracture starting point calculated by the fold catastrophe theory is the deformation value of the deterioration area, while the actual monitoring point is located at the top of the Zengziyan URM. The measured data are the total displacements (deformation values of the incompletely deterioration area and the deterioration area). Theoretically, the deformation value of the deterioration area can be converted into the total displacement by Eq. (31). But the deformation value of the incompletely deterioration area (spring) is also a function of *m*. There is a problem of error accumulation in the conversion. Therefore, we suggest that for the tower-shaped URM of compression-induced fracturing mode, the bottom deterioration area should be monitored, i.e. the monitoring points should be arranged at the top and bottom of the deterioration area to directly measure the vertical compression deformation values, and then compare their with the theoretical displacement values of the deterioration area.

Therefore, during the laboratory test, the test materials, mechanical state, boundary conditions and other conditions should be consistent with the site as much as possible to ensure that the input parameters are close to the actual situation. From the perspective of URM's monitoring and early warning, the starting point of URM fracture is the key to realizing monitoring and early warning. Because the precursor of rock collapse and fracture is not obvious, once the starting point of rock brittle fracture is reached, the rock will fail rapidly. According to the prediction method in this paper, the results of the starting point of URM fracture are conservative, but the prediction method of tower-shaped rock mass fracturing and failure based on the quantitative combination of damage catastrophe theory still has a certain reference value.

Comparing the total damage constitutive curve and total damage degree evolution curve obtained in this paper with the existing literature [38] (Fig.11), it is found that: (1) The damage constitutive curve obtained by the theoretical solution is close to the trend of the numerical simulation constitutive curve, but after entering the strain-softening stage, the strength of the theoretical solution can be 0, while the residual strength exists in the numerical simulation. (2) The trend of the damage evolution curve obtained by the theoretical solution is consistent with that of the numerical simulation, but after entering the strain-softening stage, the total damage degree of the theoretical solution can reach 1, while a high and stable total damage degree exists in the numerical simulation.

The reason for this difference is that the total damage constitutive equation (Eq. (18)) proposed in this paper is a negative exponential function based on Weibull's distribution law. When the strain reaches a specific value, the rock mass strength will tend to be 0. The numerical simulation considers the low-level acoustic emission activity in the residual failure process. Although the compression-induced fracturing occurs in the rock mass, the acoustic emission activity does not completely disappear. The acoustic emission corresponds to the rock fracture, which means that the fracture still occurs sometimes. The total damage degree equation (Eq. (19)) proposed in this paper has a similar law.

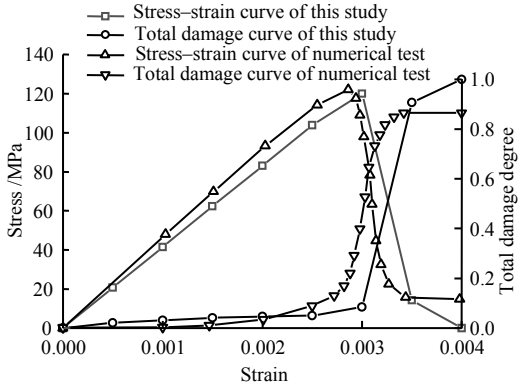

Fig. 11 Constitutive curves of total damage and evolution curve of total damage degree

6 Conclusions

Based on the case of Zengziyan rock collapse in Nanchuan District, Chongqing, a geomechanical model considering the influence of load and water-weakening effect is constructed. The damage constitutive equation and the analytical expression of the total damage degree under the coupling of multiple factors are derived by introducing the strain equivalence principle. The water-weakening function is improved. The mechanical model is generalized into an equivalent spring model, and the total potential energy function of the system is constructed based on the energy balance principle. Combining with the fold catastrophe model, the system instability criterion and the characteristic value of catastrophe displacement are obtained, and the fracturing and failure prediction model of the tower-shaped URM based on the coupling of damage and catastrophe theory is obtained. The main conclusions are drawn as follows:

(1) By introducing the Lemaitre's strain equivalence principle, general forms of damage constitutive equation and total damage degree evolution equation under multi-factor coupling are obtained. The damage constitutive equation, total damage degree evolution equation and Weibull's double-parameter analytical formula of limestone under the coupling of load and water-weakening are derived. The water-weakening function is improved to the univariate cubic function of softening coefficient.

(2) Based on the geomechanical model of fracturing and failure of the tower-shaped URM, it is simplified to the equivalent spring model under uniaxial compression, and the system fracturing and failure criterion and deterioration process under the coupling of "damage mechanics, energy method and fold catastrophe model" are obtained. The calculation shows that when the compression-induced fracturing and failure appears in the URM #W12, the control variable of fold catastrophe model is $a = -0.003251 < 0$, and the system is in an unstable state. The theoretical values of the fracture starting point, fracture ending point, and origin-destination distance are less than the measured values. The absolute error accuracies of the fracture ending point and origin-destination distance are at cm level. The absolute error accuracy of the rupture starting point is at mm level, indicating that the theoretical results are safe.

(3) The theoretical damage constitutive curve and theoretical damage evolution curve are consistent with the numerical counterparts in the existing literature, which shows that the analytical method in this paper is reasonable.

(4) The damage mechanics theoretically integrates with fold catastrophe model by energy method. The fracturing and failure mechanism of the tower-shaped rock mass is interpreted from the mechanical perspective of system catastrophe instability caused by damage evolution and accumulation, which provides a feasible theoretical method for monitoring and early warning of URM collapse in the limestone areas. In the next step, we will carry out coupling research with other catastrophe models and focus on the development of a three-dimensional stability analysis method and instability prediction of catastrophe caused by URM collapse damage. This paper puts forward the viewpoints of the loading and unloading mechanisms in the incomplete deterioration area of the equivalent spring model of a tower-shaped URM. Limited by the length of the paper, only assumptions are introduced. This part will be discussed in another article. Meanwhile, a relevant experimental research is carrying out on the optimized calculation method of the water-weakening function proposed in this paper.

References

[1] FENG Z, LI B, YIN Y P, et al. Rockslides on limestone cliffs with sub-horizontal bedding in the southwestern calcareous area, China[J]. Natural Hazards and Earth System Sciences, 2014, 14(9): 2627–2635.

[2] CHEN Hong-kai, QIN Xin. Status que and trend of unstable rock stability analysis[J]. Journal of Chongqing Jiaotong University(Natural Science), 2018, 37(10): 49–60.

[3] HE Xiao, CHEN Hong-kai, TANG Hong-mei, et al. Research on the mechanism of the development of unstable rocks in the limestone area in the Three Gorges and stability analysis for the rocks[J]. Journal of Southwest University(Natural Science Edition), 2014, 36(6): 155–160.

[4] TANG Hong-mei, ZHANG Xu-chen, WANG Lin-feng, et al. Study on the landforms evolution of high cliff in limestone area: taking Zhenziyan cliff of Jinfo mountain in Chongqing city as an example[J]. Journal of Chongqing Normal University(Natural Science), 2018, 35(5): 54–62.

[5] TANG Hong-mei, SHU Qing-jiang, WANG Lin-feng. Reliability analysis of perilous toppling rock considering seismic force direction[J]. Applied Mathematics and Mechanics, 2020, 41(3): 319–328.

[6] HE Kai, CHEN Chun-li, FENG Zhen, et al. A review on the collapse hazards of tower-shaped rock[J]. Journal of Geomechanics, 2016, 22(3): 714–724.

[7] FRAYSSINES M, HANTZ D. Failure mechanisms and triggering factors in calcareous cliffs of the subalpine ranges (French Alps.)[J]. Engineering Geology, 2006, 86(4): 256–270.

[8] FRAYSSINES M, HANTZ D. Modelling and back-analysing failures in steep limestone cliffs[J]. International Journal of Rock Mechanics & Mining Sciences, 2009, (46): 1115–1123.

[9] CARINE D P, MARC W, DENIS J, et al. Investigation of a fractured limestone cliff (chartreuse massif, france) using seismic tomography and ground-penetrating radar[J]. Near Surface Geophysics, 2003(4): 161–170.

[10] OZTEKIN B, TOPAL T, KOLAT C. Assessment of degradation and stability of a cut slope in limestone, Ankara-turkey[J]. Engineering Geology, 2006, 84(1): 12–30.

[11] POWELL W J. Exploration of the Colorado river of the west and its tributaries[M]. Washington D C: Government Printing Office, 1875.

[12] TERZAGHI K. Mechanism of landslides[M]. Berkey: Engineering Geology, The Geological Society of America, 1950: 83–123.

[13] POISEL R, ANGERER H, PÖLLINGER M, et al. Mechanics and velocity of the Lärchberg–Galgenwald landslide (Austria)[J]. Engineering Geology, 2009, 109(1): 57–66.

[14] CHEN Hong-kai, WANG Sheng-juan. Study on failure model of Wangxia perilous rock and its mechanical interpretation[J]. Journal of Chongqing Normal University (Natural Science), 2018, 35(1): 48–55.

[15] HUANG Bo-lin, YIN Yue-ping, LI Bin, et al. Simplified numerical model and verification for the impulse wave generated by situated collapse of a dangerous columnar rock mass[J]. Rock and Soil Mechanics, 2021, 42(8): 2269–2278.

[16] ZHANG Quan, HUANG Bo-lin, ZHENG Jia-hao, et al. Prediction and analysis of surge generated by crushing failure collapse of columnar dangerous rock mass[J]. Rock and Soil Mechanics, 2021, 42(10): 2845–2854.

[17] LIU Chen, YU Qing-yang, WANG Cheng-bin, et al. Deterioration law of limestone freeze-thaw cycles[J]. Exploration Engineering (Rock & Soil Drilling and Tunneling), 2019, 46(12): 80–85.

[18] HE Kai, GAO Yang, YIN Yue-ping, et al. Stability assessment methods for huge high-steep unstable rock mass based on damage theory[J]. Hydrogeology & Engineering Geology, 2020, 47(4): 82–89.

[19] ZHANG J X, SHU J Q, ZHANG H B, et al. Study on rock mass stability criterion based on catastrophe theory[J]. Mathematical Problems in Engineering, 2014, 2015: 1–8.

[20] CHANG Y, CHANG L S, REN F Q. Energy catastrophe of jointed rock slope considering spatiotemporal variability of strength[J]. Geotechnical and Geological Engineering, 2020, (39): 2547–2564.

[21] ZHOU Zi-han, CHEN Zhong-hui, ZHANG Ling-fan, et al. Energy principle based catastrophe study of slope stability in open-pit excavation[J]. Rock and Soil Mechanics, 2019, 40(12): 4881–4889.

[22] LIU Xuan-ting, CHEN Cong-xin, LIU Xiu-min, et al. Analysis of catastrophic instability of roof-rib pillar support system under backfill mining[J]. Rock and Soil Mechanics, 2021, 42(9): 2461–2471.

[23] XIA Kai-zong, LIU Xin-min, CHEN Cong-xin, et al. Analysis of mechanism of bedding rock slope instability with catastrophe theory[J]. Rock and Soil Mechanics, 2015, 36(2): 477–486.

[24] ZHOU Zi-han, CHEN Zhong-hui, WANG Jian-ming, et al. Catastrophe analysis of open-pit slope stability under blasting load[J]. Rock and Soil Mechanics, 2020, 41(3): 849–857.

[25] XU Xiao-dong, SUN Guang-hua, YAO Xu-long, et al. A cusp catastrophe warning model for instability of backfill based on energy dissipation and release[J]. Rock and Soil Mechanics, 2020, 41(9): 3003–3012.

[26] REN You-rong, CHEN Peng, ZHANG Jun, et al. Early-warning analysis on the rockfall for Zenziyan #W12 dangerous rock mass in Nanchuan City of Chongqing[J]. The Chinese Journal of Geological Hazard and Control, 2005, 16(2): 28–31, 37.

[27] 107 Geology Team of Chongqing Bureau of Geology and Mineral Resources Exploration and Development. Geology report on bauxite deposit in Loujiashan, Sichuan[R]. Chongqing: 107 Geology Team of Chongqing Bureau of Geology and Mineral Resources Exploration and Development, 1995.

[28] LEMAITRE J. A continuous damage mechanics model for ductile fracture[J]. Journal of Engineering Materials and Technology, 1985, 107(1): 83–89.

[29] ZHANG Quan-sheng, YANG Geng-she, REN Jian-xi. New study of damage variable and constitutive equation of rock[J]. Chinese Journal of Rock Mechanics and Engineering, 2003, 22(1): 30–34.

[30] WANG Jie, LI Yang, SONG Wei-dong, et al. Analysis of damage evolution characteristic of jointed rock mass with different joint dip angles[J]. Journal of Harbin Institute of Technology, 2019, 51(8): 143–150.

[31] ZHOU Yong-li, WANG Jian-ming. The research on instability mechanism of rock slope with trailing edge cracks induced by rainfall[J]. Journal of Safety Science and Technology, 2019, 15(4): 103–108.

[32] XU Teng, REN Si-yu, FAN Cheng, et al. The rheological model of rocks with water weakening effect based on variable parameters[J]. China Science Paper, 2018, 13(1): 70–77.

[33] FENG Zhen, CHEN Yun-xia, LI Bin, et al. Failure mechanism on the Zengziyan collapse in Nanchuan of Chongqing[J]. Hydrogeology & Engineering Geology, 2016, 43(1): 50–56.

[34] PAN Yue, LI Ai-wu. Discussion of potencial function and equilibrium equation about problem of rock sample monaxial compress failure[J]. Journal of Qingdao Technological University, 2008, 100(1): 1–6.

[35] WANG Zhi-qiang, WU Min-ying, PAN Yue. Fold catastrophe model of slope destabilization and its starting velocity[J]. Journal of China University of Mining & Technology, 2009, 38(2): 175–181.

[36] COOK N G W. The failure of rock[J]. International Journal of Rock Mechanics & Mining Sciences, 1965, 2(3): 389–403.

[37] 107 Geology Team of Chongqing Bureau of Geology and Mineral Resources Exploration and Development. Construction drawing design of W29 and W23 unstable rock mass treatment project of Zengzi rock mass, Jinfo mountain, Nanchuan District, Chongqing[R]. Chongqing: 107 Geology Team of Chongqing Bureau of Geology and Mineral Resources Exploration and Development, 2015.

[38] HE Kai, LI Bin, ZHU Sai-nan, et al. Experimental study on rock damage characteristic of the key zone for collapsed rock mass[J]. Chinese Journal of Under- ground Space and Engineering, 2018, 14(6): 1490–1497.